frontiers | Frontiers in Detector Science and Technology

TYPE Original Research
PUBLISHED 22 April 2025
DOI 10.3389/fdest.2025.1561739



OPEN ACCESS

EDITED BY
Gabriele Croci,
University of Milano-Bicocca, Italy

REVIEWED BY
Giorgio Dho,
National Laboratory of Frascati (INFN), Italy
Stefano Levorato,
National Institute of Nuclear Physics of Trieste, Italy

*CORRESPONDENCE
F. M. Brunbauer,
florian.brunbauer@cern.ch

RECEIVED 16 January 2025
ACCEPTED 10 April 2025
PUBLISHED 22 April 2025

CITATION
Brunbauer FM, Amedo P, Flöthner KJ, Gonzalez Diaz D, Janssens D, Leardini S, Lisowska M, Müller H, Oliveri E, Orlandini G, Pfeiffer D, Ropelewski L, Sauli F, Samarati J, Scharenberg L, van Stenis M and Veenhof R (2025) Primary and secondary scintillation of $CF_4$-based mixtures in low-pressure gaseous detectors.
*Front. Detect. Sci. Technol.* 3:1561739.
doi: 10.3389/fdest.2025.1561739



# Primary and secondary scintillation of $CF_4$-based mixtures in low-pressure gaseous detectors

F. M. Brunbauer[1]*, P. Amedo[2], K. J. Flöthner[1,3], D. Gonzalez Diaz[2], D. Janssens[1], S. Leardini[2], M. Lisowska[1], H. Müller[1,3], E. Oliveri[1], G. Orlandini[1], D. Pfeiffer[1,4], L. Ropelewski[1], F. Sauli[1], J. Samarati[2], L. Scharenberg[1], M. van Stenis[1] and R. Veenhof[1]

[1]European Organization for Nuclear Research (CERN), Geneve, Switzerland, [2]Instituto Galego de Física de Altas Enerxías (IGFAE), Universidade de Santiago de Compostela, Santiago de Compostela, Spain, [3]University of Bonn, Bonn, Germany, [4]European Spallation Source (ESS ERIC), Lund, Sweden

Optical readout of micro-pattern gaseous detectors relies on recording scintillation light emitted during electron avalanche multiplication with imaging sensors of high-granularity pixelated readout. It can be used in applications such as optical Time Projection Chambers for track reconstruction, low material budget beam monitoring or radiography, to name but a few. A good match between the scintillation light emission spectra and the spectral sensitivity of the recording devices is required to achieve high signal-to-noise ratios and ensure optimal acquisition parameters. Experimental requirements for operation at low or high pressures may have an impact on the scintillation spectra of gases commonly used for optical readout. We investigate the pressure dependence of scintillation light emission spectra of primary and secondary scintillation in the range of 1,000 mbar down to 25 mbar, in the wavelength range of 200 nm–800 nm. Primary scintillation spectra for different CF4-based mixtures are observed to be independent of pressure in the investigated range. A strong variation in the ratio of ultraviolet (UV) emission to visible (VIS) emission bands is observed as a function of pressure for secondary scintillation of $CF_4$ and He/$CF_4$ mixtures while for Ar/$CF_4$ the overall light yield varies with an almost constant ratio between UV and VIS components. While the addition of low fractions of $SF_6$ as electronegative drift gas does significantly lower the total light output, the shape of the emission spectra is not affected. The observed increase in relative UV emission for low pressure operation in $CF_4$ and He/$CF_4$ mixtures can guide the selection of optical readout devices or wavelength shifters for applications requiring low gas pressure operation.

KEYWORDS

**gaseous detector, scintillation, optical readout, MPGD (Micropattern gaseous detector), CF4**

# 1 Introduction

The optical readout of gaseous radiation detectors allows to use state-of-the-art imaging sensors to acquire high-granularity images representing incident radiation. MicroPattern Gaseous Detector (MPGD) technologies including Gaseous Electron Multipliers (GEMs) and MicroMesh Gaseous Structures (Micromegas) can be used as amplification structures producing significant scintillation light that is recorded with solid state imaging sensors like CCD and CMOS devices or fast photon detectors including Photomuliplier Tubes (PMTs) or Silicon Photomultipliers (SiPMs) with time resolutions on the order of nanoseconds. Advantages of optical readout include the high pixel count of modern cameras which allows for high spatial resolution imaging, the flexibility to tune magnification and guide light with suitable optical elements including lenses and mirrors, insensitivity to electronic noise and decoupling between readout and amplification structures. On the other hand, the low frame rate on the order of hundreds of Hz to kHz of most imaging sensors limits optical readout with CCD and CMOS sensors to an integrated imaging approach or makes it suitable only for low event rate environments. This limitation is gradually being overcome by the development of novel high-speed CMOS sensors and cameras based on Timepix ASICs. To be compatible with the spectral sensitivity of most commercially available cameras, optical readout is predominantly performed with gas mixtures containing carbon tetrafluoride ($CF_4$) which features ample visible-range scintillation light emission (Fraga et al., 2003). The requirement for visible scintillation light emission to assure compatibility with common imaging sensors has led to the majority of optically read out gaseous detectors relying on $CF_4$ or gas mixtures of noble gases and $CF_4$. Optically read out detectors using $CF_4$-based gas mixtures and MPGD-based amplification structures are used for track reconstruction in optical Time Projection Chambers (TPCs) including the MIGDAL (Araújo et al., 2023) and CYGNO experiments (Amaro et al., 2022) and have been shown to allow for detailed event reconstruction. Scintillation light emission yields in the wavelength range compatible with the employed imaging sensor plays a crucial role in achieving high signal-to-noise ratios in optically read out detectors. Therefore, a detailed understanding of the emission spectra of different gas mixtures as a function of operating conditions, including gas pressure and electric field, is important. The effect of varying electric field and pressure on $CF_4$ spectral shapes and light yields has been studied for ambient and high pressures with $\alpha$ tracks (Morozov et al., 2010; Morozov et al., 2011) and a relative increase of VIS emission with respect to UV emission has been observed for low electric field as well as for higher pressures, which can be explained by an increasing probability for recombination in these mixtures leading to visible emission from $CF_3$* states (Morozov et al., 2010). While high gas pressure can be imperative in applications requiring high target density for increasing interaction/decay probability or event containment, low-pressure operation can be advantageous for reconstructing low energy events due to the longer track lengths. An example is the MIGDAL experiment, operating a low-pressure TPC for reconstructing low energy electron tracks with a hybrid electronic and optical readout technique (Araújo et al., 2023; Brunbauer et al., 2018). We studied the variation of primary and secondary scintillation spectra of $CF_4$-based mixtures in low pressure conditions from ambient pressure down to 25 mbar in the UV-VIS-near-infrared (NIR) range (200 nm–800 nm) relevant for optical readout applications including pure $CF_4$, $Ar/CF_4$, $He/CF_4$ and tertiary mixtures containing $SF_6$ for negative ion drift. Negative ion drift is attractive for TPCs as it strongly reduces diffusion (Martoff et al., 2000; Ohnuki et al., 2001) and can be used to improve the spatial resolution. $SF_6$ has received attention as negative ion drift gas due to its ease of use, its electro-negativity and its prevalence in high voltage insulation and numerous other industrial applications. It is proposed as negative ion drift gas for directional dark matter experiments (Phan et al., 2017; Ikeda et al., 2020; Amaro et al., 2024) and other TPC developments and applications (Ligtenberg et al., 2021).

# 2 Experimental setup

Spectroscopic measurements of primary and secondary scintillation were performed in two setups: a gas volume with a collimating lens for primary scintillation and a GEM-based TPC for secondary scintillation.

Primary scintillation was recorded by collecting light emitted in a 10 cm thick gas volume with a collimating lens. X-rays from a Cu target X-ray generator operated at 40 kV with 38 mA filament current were used to irradiate the gas volume with high flux. The volume was pumped to base pressures below $10^{-2}$ mbar and subsequently flushed with pure $CF_4$ or mixtures for at least 10 h. Gases with purity level of 45 or better were used. The initial pumping and filling procedure, as well as subsequent flushing and exchange of multiple volumes of gas, was performed to minimize contamination in the vessel, which may result from the outgassing from detector components. For the measurements, the volume was sealed and data was recorded at decreasing pressures. No electric field was applied and the setup, including the gas vessel, was grounded. An $f/2$ fused-silica collimating lens (OceanOptics 74-UV) with 5 mm diameter and 10 mm focal length, compatible with a wavelength range of 185 nm–2,500 nm, was used (74-UV).

The secondary-scintillation spectroscopy setup is shown in Figure 1. A single 10 cm × 10 cm glass GEM is placed in a TPC configuration with a 10 cm diameter, 10 cm-long field shaper and a mesh cathode. The glass GEM features 160 µm–180 µm diameter holes at a pitch of 280 um in a 570 µm-thick photo-etchable glass substrate (Takahashi et al., 2013) and was chosen for operating stably in a wide range of pressures due to the high aspect ratio of its holes which suppresses photon feedback geometrically.

The 'top' electrode of the glass GEM (cathode side) was grounded and the bottom electrode (anode side) was powered with a high-voltage supply. Current collected at the bottom electrode was recorded from the power supply and used for normalising the secondary scintillation spectra. A drift field of 50 V/cm was applied between the cathode and the top electrode of the glass GEM. All avalanche electrons were collected on the bottom electrode of the glass GEM.

X-rays from a generator (Amptek Mini-X) were introduced through a thin Al foil window at the cathode side, with a diameter of 1 cm. Spectra were acquired with 20 kV X-ray voltage and 200 µm filament current resulting in primary currents on the scale of 1–10 nA, depending on gas composition and pressure. A lower X-ray flux was required for secondary scintillation measurements compared to the

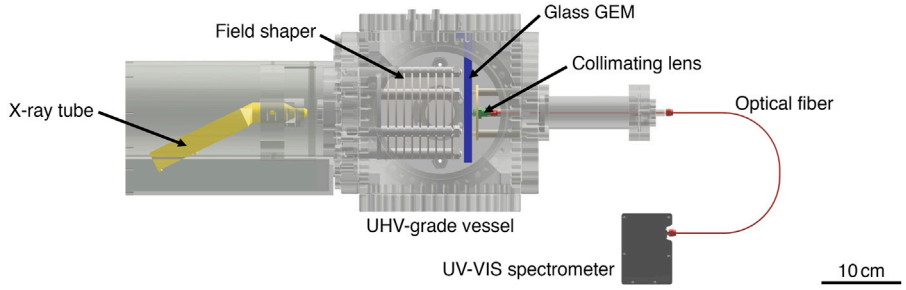


FIGURE 1
Spectroscopy setup for secondary scintillation measurements: a single glass GEM is used as electron amplification structure in a TPC-like detector setup contained in a UHV-grade gas volume. An X-ray tube is irradiating the chamber through a thin foil window and a mesh cathode from the left. A collimating lens placed below the GEM is collecting scintillation light into an optical fiber. Light is guided through a feedthrough to the UV-VIS spectrometer located outside of the detector volume.

primary scintillation measurements due to the gain of the amplification stage.

A fiber-coupled CCD spectrometer (Ocean Optics FLAME S UV-VIS) with a 200 µm entrance slit was used. Light was coupled with a 5 mm diameter UV-VIS collimating lens and two optical fibers connected with a fiber feedthrough, one vacuum-compatible fiber inside the gas volume and a standard multi-mode fiber outside the gas volume.

For primary and secondary scintillation measurements, spectra were recorded with an exposure time of 30 s and multiple spectra were averaged for each data point. Background spectra were recorded without X-ray irradiation and with the detector powered off. Multiple background spectrum acquisitions were averaged and subtracted from the data.

For primary and secondary scintillation measurements, spectra were corrected for the spectral response and wavelength-dependent transmission of setup elements including the collimating lens, optical fibers and the fiber feedthrough. A UV-VIS-NIR calibration light source (Ocean Optics DH-3plus-CAL) was used to acquire calibration files by introducing light in the spectroscopy setup and separately comparing acquired spectra of deuterium and halogen lamps to nominal lamp output spectra.

## 3 Scintillation spectra

Scintillation spectra for pure $CF_4$, Ar/$CF_4$ and He/$CF_4$ gas mixtures were recorded as a function of pressure. Depending on the gas mixture, different lower limits of pressure could be reached where the detector could not be operated in stable conditions. Secondary scintillation spectra are provided as photon flux divided by the number of secondary electrons as a function of wavelength, the photon flux not being absolutely normalized. Primary scintillation spectra are also given as photon flux but are not divided by the number of electrons.

### 3.1 Primary scintillation

A comparison of primary scintillation spectra of $CF_4$, Ar/$CF_4$ and He/$CF_4$ at ambient pressure without electric field is shown in Figure 2. For the gas mixtures, a mixing ratio of 80/20% by volume was chosen, which is a common choice in optical readout applications. While UV emission bands are present in all the mixtures studied, no observable emission band centered around 630 nm is present in He/$CF_4$ 80/20%. The primary scintillation spectra are not normalised and the total light yield cannot be compared for the different mixtures. However, the relative intensity between VIS and UV emission bands displays a clear dependence with the gas mixture, with Ar/$CF_4$ exhibiting significantly stronger VIS scintillation compared to pure $CF_4$ and He/$CF_4$ exhibiting a weaker one.

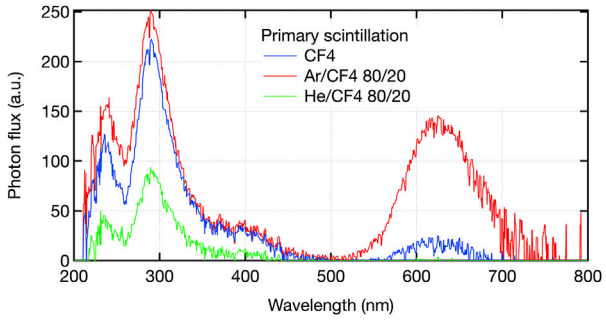


FIGURE 2
Primary scintillation spectra of $CF_4$, Ar/$CF_4$ and He/$CF_4$ gas mixtures: UV emission bands are present in all three mixtures with comparable ratios between peaks. The visible scintillation band measured for Ar/$CF_4$ and pure $CF_4$ is not observed for He/$CF_4$.

The UV and VIS emission bands of $CF_4$ are resulting from emission from different molecules that can be created by direct excitation as a result of the fragmentation of $CF_4$ molecules. $CF_3^*$ is responsible for the visible emission band centered around 630 nm while the UV emission between 200 nm and 450 nm is attributed to excited states of the ion $CF_4^+$ (Morozov et al., 2011). Recombination effects may lead to the neutralisation of $CF_4^+$ and $CF_3^+$ ions and create additional VIS emission from $CF_3^*$. The UV emission band features distinctive features for all three gases: a main peak at 290nm, a second peak around 240 nm and a shoulder around 400 nm, which can be attributed to the $CF_4^+\tilde{D} \rightarrow CF_4^+\tilde{C}$ transition Lambert et al. (1988). The emission peaks at 220 nm and 290 nm may be assigned

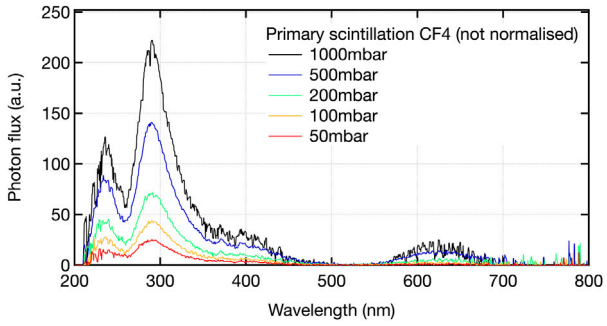


FIGURE 3
Primary scintillation spectra of pure $CF_4$ as function of pressure: UV and VIS emission bands are observed with the same ratio for pressures from 1,000 mbar to 50 mbar.

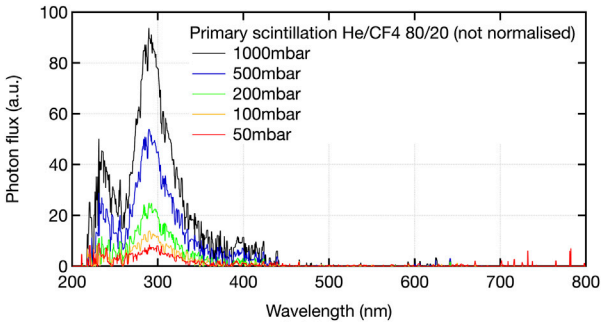


FIGURE 5
Primary scintillation spectra of He/$CF_4$ (80/20%) as function of pressure: only UV emission bands are observed, and the shape remains largely unchanged, except perhaps at 50 mbar where the 230 nm band shows a similar amplitude as the 290 nm one.

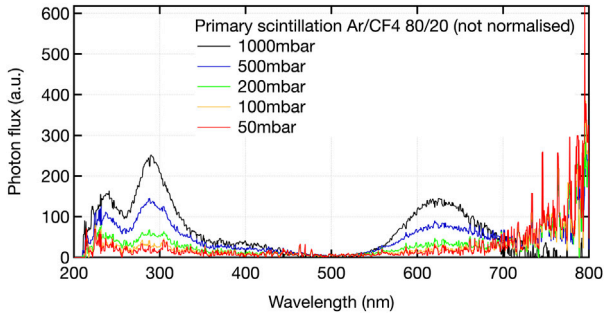


FIGURE 4
Primary scintillation spectra of Ar/$CF_4$ (80/20%) as a function of pressure: UV and VIS emission bands are observed with the same ratio for pressures from 1,000 mbar to 50 mbar. The spectral shapes in the UV region (in particular the ratio between the 240 nm and 290 nm peaks) appear slightly modified below 200 mbar.

to $CF_4^+\tilde{C} \rightarrow CF_4^+\tilde{X}$ and $CF_4^+\tilde{C} \rightarrow CF_4^+\tilde{A}$, respectively (Lambert et al., 1988). Other studies comparing the emission of different fluorocarbons observed that the peak at 240 nm appears only with $CF_4$ and may be attributed to emission from $CF_4^+$, while the peak at 290 nm appears also for other fluorocarbons and may thus have a contribution from emission from $CF_2^+$ Fanelli et al. (2008). Contrary to pure $CF_4$ or Ar/$CF_4$ mixtures, the absence of significant visible scintillation in the He/$CF_4$ gas mixture indicates that neither direct excitation, nor recombination nor wavelength-shifting transfers produce significant amounts of $CF_3^*$ precursors to feed the 630 nm band.

The primary scintillation spectra of $CF_4$ for pressures ranging from 1,000 mbar down to 50 mbar are shown in Figure 3. Spectra are not normalised to the rate of interactions and the decreasing signal amplitude is likely dominated by the lower interaction rate with decreasing gas density. Spectral features remain unchanged with decreasing pressure and the ratio of UV to VIS components remains constant. For low pressures below 200 mbar, the sensitivity of the spectrometer limits the estimation of the UV to VIS ratio.

The primary scintillation spectra of an Ar/$CF_4$ gas mixture (80/20% by volume) for pressures ranging from 1,000 mbar down to 50 mbar are shown in Figure 4. As in the case of pure $CF_4$, spectra are not normalised to the interaction rate. UV and VIS emission bands are clearly visible for higher pressures, with spectra recorded at lower pressures being limited by the sensitivity of the spectrometer. NIR emission lines attributed to direct emission from Ar states are observed for the lowest pressures.

Primary scintillation spectra of an He/$CF_4$ gas mixture (80/20% by volume), for pressures ranging from 1,000 mbar down to 50 mbar, are shown in Figure 5. As in the case of pure $CF_4$, spectra are not normalised to the interaction rate. Only UV emission peaks at 230 nm and 290 nm and a shoulder around 400 nm are present, as previously. The ratio of the intensity of the 290 nm emission peak to the 230 nm emission peak remains approximately constant at 2.3 ± 0.3. The VIS emission band is absent for all pressures.

The absence of strong pressure dependencies of the spectral shapes in the range corresponding to the $CF_4$ bands, as observed here for X-rays in $CF_4$, Ar/$CF_4$ and He/$CF_4$ mixtures in the pressure regime from 1,000 mbar down to 50 mbar, is well in line with observations made earlier for Ar/$CF_4$ mixtures in the pressure regime 1–5 bar (Amedo et al., 2023). Thus, it may be inferred that the mechanisms leading to the formation of the UV and VIS scintillation precursors from X-ray interactions evolve with pressure in a similar way, as far as primary scintillation is concerned, from 50 mbar possibly up to 5 bar, at least.

## 3.2 Secondary scintillation

Secondary scintillation spectra were recorded with a glass GEM in a TPC setup as shown in Figure 1. Spectra are normalised in this case to the total collected current after electron multiplication. The detector was operated at voltages where some saturation of the gain was observed, hinting at possible space-charge effects. The effect of the operation in a regime with some loss of linearity was examined for different drift field strengths from 50 V/cm to 100 V/cm, for GEM gain values from several 10s–1000s and for varying X-ray flux. Operating with different parameters, the normalisation of recorded spectra by collected secondary current exhibited variations of up to 10% while the overall features of the spectra and the relative

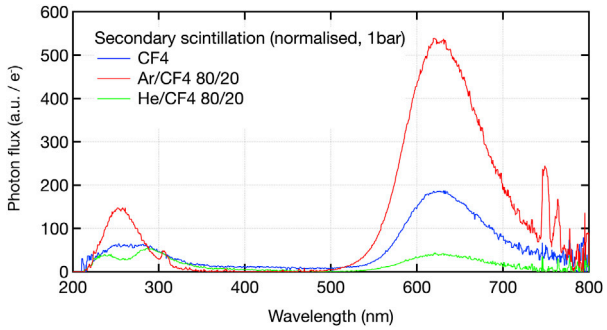


FIGURE 6
Secondary scintillation spectra of $CF_4$, Ar/$CF_4$ and He/$CF_4$ gas mixtures: scintillation strength normalised to collected current. UV and VIS emission bands are observed for all three mixtures. Ar/$CF_4$ displays the characteristic emission lines from Ar in the NIR range.

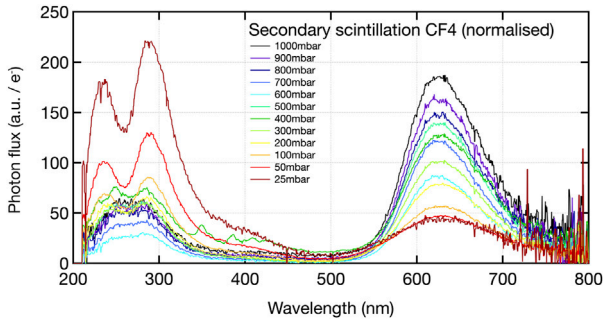


FIGURE 7
Secondary scintillation spectra of $CF_4$ as function of pressure: scintillation strength normalised to collected current close to maximum stable gain.

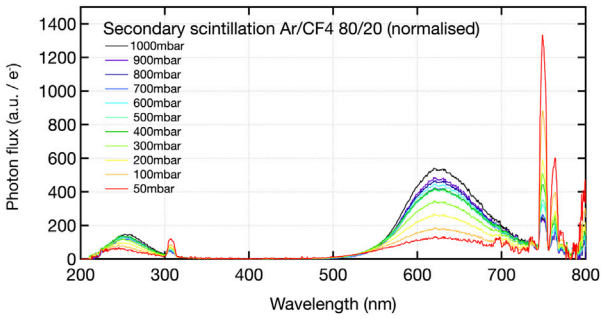


FIGURE 8
Secondary scintillation spectra of Ar/$CF_4$ as function of pressure: scintillation strength normalised to collected current close to maximum stable gain.

amplitude of different emission bands and features were not affected.

A comparison of the secondary scintillation spectra of $CF_4$, Ar/$CF_4$ and He/$CF_4$ at 1,000 mbar, normalised to the collected electron current, is shown in Figure 6. While no absolute photon flux can be provided, the normalised spectra can be used to compare the relative scintillation strengths of the different gas mixtures. The high light yield of Ar/$CF_4$ compared to He/$CF_4$ agrees with previous quantitative measurements reported for GEM detectors (Fraga et al., 2003), where higher optical gains were observed for Ar-based mixtures compared to He-based, at the same avalanche gain. On the other hand, the UV band in Figure 6 hints at the presence of an additional peak at around 260 nm, pressumably stemming from the decay $CF_3^*(2A_1') \rightarrow CF_3(1A_2'')$, Amedo et al. (2023). It is much more prominent in case of Ar mixtures, but its presence can be hinted in case of secondary scintillation for all mixtures, as the peak-to-valley ratio for any of the two main UV peaks gets reduced compared to that observed in the primary scintillation.

Secondary scintillation spectra in pure $CF_4$ for pressures ranging from 1,000 mbar to 25 mbar are shown in Figure 7. The electric field across the glass GEM was varied from 43 kV/cm at 1,000 mbar to 10 kV/cm at 25 mbar. While abundant light emission is observed across the full range of pressures, a significant shift from the VIS to the UV emission band is observed with decreasing pressure. Further, the shape of the UV band also changes, making more apparent the contribution of the $CF_3^*$ peak at 260 nm.

The above observations can be correlated with the fact that avalanche multiplication at low pressure takes place at higher values of the pressure-reduced electric field, implying higher energy of the electrons within the avalanche. The higher electron energy needed to produce $CF_4^{+,*}$ states compared to that needed for $CF_3^*$ (Amedo et al., 2023) can explain qualitatively the changes observed in the spectra as the pressure is reduced. It cannot be completely excluded that this trend reflects partly the appearance of $CF_3^*$ from electron-ion recombination inside the holes, as reported earlier for primary ionization in the range 2 – 5 bar (Morozov et al., 2011). However, the different pressure-dependence of the spectra of emission of $CF_4$, Ar/$CF_4$ and He/$CF_4$ (as discussed below) suggests that this, if present, cannot be the dominant mechanism leading to the suppression of $CF_3^*$ production as pressure decreases.

The observed modifications, specifically the decrease of visible light emission yield, have important implications for detectors operating at low pressures such as the optical TPC used in the MIGDAL experiment operating at 50 torr of pure $CF_4$ (Araújo et al., 2023). In those conditions, imaging sensors with suitable spectral responsivity have to be chosen to achieve good signal-to-noise ratios or solid wavelength shifting employed.

In Ar/$CF_4$ (80/20%) a different behavior of the emission bands with decreasing pressure is observed, with a constant ratio between the visible and UV emission bands as shown in Figure 8. Also, a single UV emission peak is observed across pressures, that points to the insufficient electron energy to produce $CF_4^{+,*}$ in Ar-based mixtures, in the pressure range studied. For the measurements, the electric field across the glass GEM was varied from 29 kV/cm at 1,000 mbar to 6.6 kV/cm at 25 mbar.

The overall scintillation strength in the $CF_3^*$ bands decreases for lower pressures, while the Ar atomic lines attributed to transitions between Ar states with electronic configurations (3p5 4p) and (3p5 4s) become more prominent (Fraga et al., 2003). The increase of IR emission can be correlated with the larger electron energy at low pressures as well as the reduced effect of self-quenching of IR

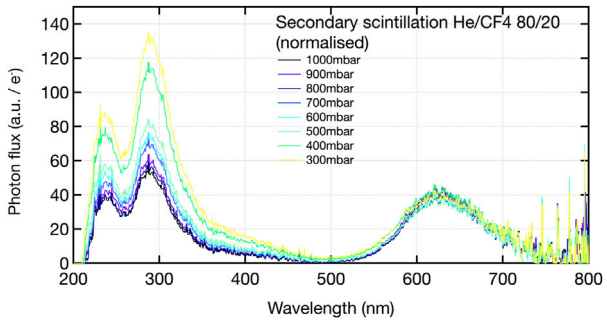


FIGURE 9
Secondary scintillation spectra of $He/CF_4$ as function of pressure: scintillation strength normalised to collected current close to maximum stable gain.

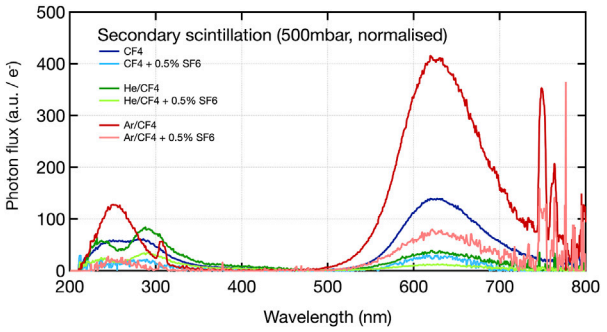


FIGURE 11
Secondary scintillation spectra of $CF_4$, $Ar/CF_4$ and $He/CF_4$ at 500 mbar total pressure, without and with the addition of 0.5% $SF_6$.

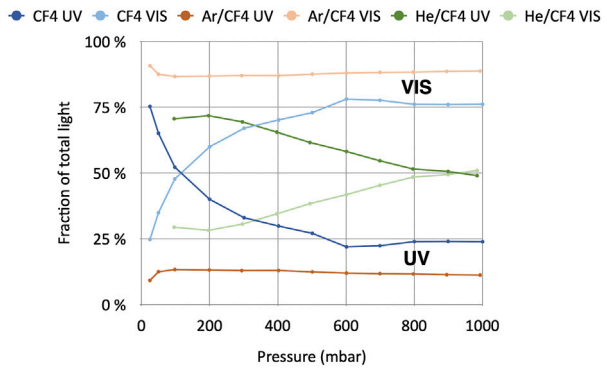


FIGURE 10
Fraction of UV and VIS emission components of the secondary scintillation spectra of $CF_4$, $Ar/CF_4$ (80/20%) and $He/CF_4$ (80/20%). The UV intensity was determined by integrating spectra from 200 nm to 500 nm; while the wavelength range from 500 nm to 800 nm was integrated for the VIS intensity.

precursors ($Ar^{**}$) with Ar neutral atoms, as observed in (Amedo et al., 2023). The overall decrease of the $CF_3^*$ emission bands suggests that charge-transfer processes between Ar and $CF_4$ start to become suppressed below atmospheric pressure.

Finally it must be noted that a narrow emission peak around 310 nm is observed for all $Ar/CF_4$ spectra, which can be attributed to emission from OH* (Mašláni and Sember, 2014). The level of water in the $Ar/CF_4$ was comparable to the level in other investigated mixtures. The noticeable peak at 310 nm might be attributed to the existence of significant cross-sections for populating the OH* state in this gas mixture, as indicated in (Amedo et al., 2023).

Secondary scintillation spectra of $He/CF_4$ (80/20%) for pressures ranging from 1,000 mbar to 300 mbar are shown in Figure 9. The electric field across the glass GEM was varied from 18.7 kV/cm at 1,000 mbar to 8 kV/cm at 50 mbar.

In contrast to the primary scintillation spectra of these gas mixtures as shown in Figure 5, the visible scintillation band of $CF_3$* is very apparent here. Yields are much lower than in the Ar case, though. An increase of the UV band as pressure decreases is observed, that might be again the result of a higher electron energy as pressure is reduced, resulting in a higher production of $CF_4^{+,*}$. Given that transfer reactions leading to $CF_3^*$ do not seem to be present in this mixture, as extracted from the primary scintillation spectra, one might expect them to be absent in avalanche conditions too. If such would be the case, the natural conclusion to extract from the spectral shapes in $He/CF_4$ is that, in this situation, the direct production of $CF_3^*$ is more likely when the medium is excited bottom-up (avalanche) compared to top-down (X-ray radiation).

The trends of the VIS and UV fractions of the total light intensity in $CF_4$, $Ar/CF_4$ and $He/CF_4$ are compiled in Figure 10. A cut-off wavelength of 500 nm was assumed, in order to differentiate between the UV and VIS components, and the intensity in the short and long wavelength regions was integrated and normalised to the overall integral of the full spectra. While this does not reflect variations in the total light intensity emitted, the trend to increased UV emission for pure $CF_4$ and $He/CF_4$ is noticeable in contrast to the stable ratio between emission bands for $Ar/CF_4$.

## 3.3 Secondary scintillation with negative ion drift

In addition to the electron-drift gas mixtures such as $CF_4$, $Ar/CF_4$ and $He/CF_4$ commonly used for optical readout, the effect of the addition of small quantities of the electronegative gas $SF_6$, where the charge carriers are negative ions formed in the radiation interactions (so-called negative ions gas), was examined. The secondary scintillation spectra of $CF_4$, $Ar/CF_4$ and $He/CF_4$ without and with the addition of 0.5% $SF_6$ are shown in Figure 11. Spectra are normalised to the total current collected at the bottom electrode of the GEM. The maximum achieved gain with the addition of $SF_6$ was significantly lower with the maximum scintillation strength lower by about a factor of 5x at the maximum stable charge gain.

For all mixtures, the same features are visible in the secondary scintillation spectra with and without $SF_6$. In mixtures containing $SF_6$, the overall intensity of scintillation light is significantly lower, which may be explained by $SF_6$-induced quenching of the CF4 scintillator precursors. The same trend of UV and VIS

fractions as a function of pressure shown in Figure 10 for standard electron drift mixtures was observed for mixtures containing $SF_6$.

Further and more systematic studies of the impact of the admixture of negative-ion gases to scintillating gas mixtures will be investigated, including the effect of varying pressures and electric field. This is of great relevance in view of the potential of optically read out negative ion TPCs, owing to the decreased diffusion and low drift velocities potentially enabling high-resolution 3D track reconstruction.

## 4 Conclusion

Primary and secondary scintillation spectra of gas mixtures commonly used for optically read out MPGDs were investigated, in particular their variations with electric field, for sub-atmospheric pressures. While the shapes of the primary scintillation spectra are almost unaffected by pressure variations, significant spectral modifications were found for secondary scintillation spectra, most importantly altering the ratios of the UV/VIS scintillation, that is crucial for optical readout. The general trend observed, for both $CF_4$ and $He/CF_4$, was the enhancement of the UV emission as pressure decreased, while the ratio of UV and VIS components remained approximately constant for $Ar/CF_4$. This can be expected to have implications on the choice of readout devices for detectors operating with these mixtures at low pressure. To exploit the UV part of the spectra, UV-sensitive image sensors may be used or wavelength shifting layers may be employed, to re-emit light at longer wavelengths compatible with visible-sensitive imaging sensors.

In addition, the impact on the scintillation spectra of adding a small amount of $SF_6$, in order to enable a negative-ion drift detector, was investigated. The reduced light yield per secondary electron created during avalanche multiplication seems to impose the use of high-sensitivity imaging sensors and/or image intensifiers for optically read out negative ion TPCs. Qualitatively, the scintillation-spectra features are almost unaffected by the addition of $SF_6$, however.

The presented study for $CF_4$-based gases may be used to choose optimal readout devices for optically read out MPGDs at sub-atmospheric pressures. In order to minimise the dependence of $CF_4$ as a scintillation gas, spectroscopic studies of alternative gas mixtures are needed to understand the possibilities for imaging with sensors featuring extended sensitivity ranges, ideally avoiding the use of solid wavelength shifters.

## Data availability statement

The raw data supporting the conclusions of this article will be made available by the authors, without undue reservation.

## Author contributions

FB: Conceptualization, Data curation, Formal Analysis, Investigation, Methodology, Supervision, Validation, Visualization, Writing – original draft, Writing – review and editing. PA: Conceptualization, Investigation, Writing – review and editing. KF: Conceptualization, Investigation, Writing – review and editing. DD: Conceptualization, Investigation, Supervision, Writing – review and editing. DJ: Conceptualization, Investigation, Writing – review and editing. SL: Conceptualization, Data curation, Investigation, Writing – review and editing. ML: Conceptualization, Investigation, Writing – review and editing. HM: Conceptualization, Writing – review and editing. EO: Conceptualization, Supervision, Writing – review and editing. GO: Writing – review and editing. DP: Writing – review and editing. LR: Conceptualization, Supervision, Writing – review and editing. FS: Conceptualization, Writing – review and editing. JS: Conceptualization, Writing – review and editing. LS: Conceptualization, Writing – review and editing. MV: Conceptualization, Writing – review and editing. RV: Conceptualization, Writing – review and editing.

## Funding

The author(s) declare that no financial support was received for the research and/or publication of this article.

## Conflict of interest

The authors declare that the research was conducted in the absence of any commercial or financial relationships that could be construed as a potential conflict of interest.

The author(s) declared that they were an editorial board member of Frontiers, at the time of submission. This had no impact on the peer review process and the final decision.

## Generative AI statement

The author(s) declare that no Generative AI was used in the creation of this manuscript.

## Publisher's note



## References

Amaro, F., Baracchini, E., Benussi, L., Bianco, S., Borra, F., Capoccia, C., et al. (2024). Charge amplification in low pressure cf4:sf6:he mixtures with a multi-mesh thgem for directional dark matter searches. *J. Instrum.* 19, P06021. doi:10.1088/1748-0221/19/06/P06021

Amaro, F. D., Baracchini, E., Benussi, L., Bianco, S., Capoccia, C., Caponero, M., et al. (2022). The CYGNO experiment. *Instruments* 6, 6. doi:10.3390/instruments6010006

Amedo, P., González-Díaz, D., Brunbauer, F. M., Fernández-Posada, D. J., Oliveri, E., and Ropelewski, L. (2023). Observation of strong wavelength-shifting in the argon-tetrafluoromethane system. *Front. Detect. Sci. Technol.* 1. doi:10.3389/fdest.2023.1282854

Araújo, H. m., Balashov, S., Borg, J., Brunbauer, F., Cazzaniga, C., Frost, C., et al. (2023). The MIGDAL experiment: measuring a rare atomic process to aid the search for dark matter. *Astropart. Phys.* 151, 102853. doi:10.1016/j.astropartphys.2023.102853

Brunbauer, F. M., Garcia, F., Korkalainen, T., Lugstein, A., Lupberger, M., Oliveri, E., et al. (2018). Combined optical and electronic readout for event reconstruction in a GEM-based TPC. *IEEE Trans. Nucl. Sci.* 65, 913–918. doi:10.1109/TNS.2018.2800775

Fanelli, F., Fracassi, F., and d'Agostino, R. (2008). Fluorination of polymers by means of He/CF4-fed atmospheric pressure glow dielectric barrier discharges. *Plasma Process. Polym.* 5, 424–432. doi:10.1002/ppap.200800012

Fraga, M., Fraga, F., Fetal, S., Margato, L., Marques, R., and Policarpo, A. (2003). The GEM scintillation in He–CF4, Ar–CF4, Ar–TEA and Xe–TEA mixtures. *Nucl. Instrum. Methods Phys. Res. Sect. A Accel. Spectrom. Detect. Assoc. Equip.* 504, 88–92. doi:10.1016/S0168-9002(03)00758-7

Ikeda, T., Shimada, T., Ishiura, H., Nakamura, K., Nakamura, T., and Miuchi, K. (2020). Development of a negative ion micro tpc detector with sf6 gas for the directional dark matter search. *J. Instrum.* 15, P07015. doi:10.1088/1748-0221/15/07/P07015

Lambert, I. R., Mason, S. M., Tuckett, R. P., and Hopkirk, A. (1988). Decay pathways of excited electronic states of Group IV tetrafluoro and tetrachloro molecular ions studied with synchrotron radiation. *J. Chem. Phys.* 89, 2683–2690. doi:10.1063/1.455019

Ligtenberg, C., van Beuzekom, M., Bilevych, Y., Desch, K., van der Graaf, H., Hartjes, F., et al. (2021). On the properties of a negative-ion tpc prototype with gridpix readout. *Nucl. Instrum. Methods Phys. Res. Sect. A Accel. Spectrom. Detect. Assoc. Equip.* 1014, 165706. doi:10.1016/j.nima.2021.165706

Martoff, C., Snowden-Ifft, D., Ohnuki, T., Spooner, N., and Lehner, M. (2000). Suppressing drift chamber diffusion without magnetic field. *Nucl. Instrum. Methods Phys. Res. Sect. A Accel. Spectrom. Detect. Assoc. Equip.* 440, 355–359. doi:10.1016/S0168-9002(99)00955-9

Mašláni, A., and Sember, V. (2014). Emission spectroscopy of OH radical in water-argon arc plasma jet. *J. Spectrosc.* 2014, 1–6. doi:10.1155/2014/952138

Morozov, A., Fraga, M., Pereira, L., Margato, L., Fetal, S., Guerard, B., et al. (2010). Photon yield for ultraviolet and visible emission from CF4 excited with -particles. *Nucl. Instrum. Methods Phys. Res. Sect. B Beam Interact. Mater. Atoms* 268, 1456–1459. doi:10.1016/j.nimb.2010.01.012

Morozov, A., Fraga, M., Pereira, L., Margato, L., Fetal, S., Guerard, B., et al. (2011). Effect of the electric field on the primary scintillation from CF4. *Nucl. Instrum. Methods Phys. Res. Sect. A Accel. Spectrom. Detect. Assoc. Equip.* 628, 360–363. doi:10.1016/j.nima.2010.07.001

Ohnuki, T., Snowden-Ifft, D. P., and Martoff, C. (2001). Measurement of carbon disulfide anion diffusion in a tpc. *Nucl. Instrum. Methods Phys. Res. Sect. A Accel. Spectrom. Detect. Assoc. Equip.* 463, 142–148. doi:10.1016/S0168-9002(01)00222-4

Phan, N., Lafler, R., Lauer, R., Lee, E., Loomba, D., Matthews, J., et al. (2017). The novel properties of sf6 for directional dark matter experiments. *J. Instrum.* 12, P02012. doi:10.1088/1748-0221/12/02/P02012

Takahashi, H., Mitsuya, Y., Fujiwara, T., and Fushie, T. (2013). Development of a glass GEM. *Nucl. Instrum. Methods Phys. Res. Sect. A Accel. Spectrom. Detect. Assoc. Equip.* 724, 1–4. doi:10.1016/j.nima.2013.04.089